



## Case study

## Algorithms for extraction of structural attitudes from 3D outcrop models



Camila Duelis Viana<sup>a,\*</sup>, Arthur Endlein<sup>a</sup>, Ginaldo Ademar da Cruz Campanha<sup>a</sup>,  
Carlos Henrique Grohmann<sup>b</sup>

<sup>a</sup> Institute of Geosciences, University of São Paulo, São Paulo 05508-080, Brazil

<sup>b</sup> Institute of Energy and Environment, University of São Paulo, São Paulo 05508-010, Brazil

## ARTICLE INFO

## Article history:

Received 28 August 2015

Received in revised form

24 February 2016

Accepted 25 February 2016

Available online 27 February 2016

## Keywords:

Discontinuity analysis

Python

Close-range photogrammetry

Structure-from-motion

## ABSTRACT

The acquisition of geological attitudes on rock cuts using traditional field compass survey can be a time consuming, dangerous, or even impossible task depending on the conditions and location of outcrops. The importance of this type of data in rock-mass classifications and structural geology has led to the development of new techniques, in which the application of photogrammetric 3D digital models has had an increasing use. In this paper we present two algorithms for extraction of attitudes of geological discontinuities from virtual outcrop models: *ply2atti* and *scanline*, implemented with the Python programming language. The *ply2atti* algorithm allows for the virtual sampling of planar discontinuities appearing on the 3D model as individual exposed surfaces, while the *scanline* algorithm allows the sampling of discontinuities (surfaces and traces) along a virtual scanline. Application to digital models of a simplified test setup and a rock cut demonstrated a good correlation between the surveys undertaken using traditional field compass reading and virtual sampling on 3D digital models.

© 2016 Elsevier Ltd. All rights reserved.

## 1. Introduction

Structural attitudes of rock planar discontinuities such as joints, fractures and faults, are essential data with numerous applications, from rock-mass classification to classical structural geology. However, their acquisition by field mapping with magnetic compass measurements can be time consuming (especially in surveys for geotechnical applications when hundreds or thousands of measurements must be taken), dangerous (when performed on high slopes or unstable areas) or even impossible (e.g., in Planetary Sciences). These points have led to the development of safer, faster and more cost-efficient techniques to acquire this kind of data.

Acquisition of geological data from three-dimensional digital models has become more common in the past few years (Assali et al., 2014; Haneberg, 2008; Sturzenegger and Stead, 2009; Vasuki et al., 2014; Westoby et al., 2012). The emergence of digital photogrammetric techniques, and especially those based on Structure from Motion (SfM – Wu et al., 2011; Wu, 2013; Moulon and Bezi, 2012) can make 3D photogrammetric reconstruction of rock outcrops easier and more accessible, as they can be performed with

relatively low-cost digital cameras and on desktop computers. These advances made digital photogrammetry a valid alternative to the more expensive and complex method of terrestrial laser scanning (TLS) (Tavani et al., 2014).

Generally speaking the SfM algorithm uses a given set of partially overlapping images to automatically detect common points in image pairs and, then, calculate the camera parameters and 3D coordinates of each point, generating a sparse point-cloud. This cloud can be densified by interpolation of the initially recognized points, creating a dense point-cloud. The point-cloud can then be used to generate a triangular irregular mesh. Depending on the application both point-clouds and meshes can be resampled to generate a model with regular spacing or decimated to reduce polygon/face count and speed up processing. The generated mesh can also be used to calculate a raster Digital Elevation Model (DEM). After mesh generation, the image information is assigned to each mesh triangle using a texture map. A (U,V) coordinate is assigned to each triangle vertex, representing a point in the texture map. These coordinates allow to crop a triangle in the texture map and paste it onto the corresponding triangle of the mesh (Tavani et al., 2014).

For TLS technique, the characteristics of the equipment define the maximum detail level that can be acquired. In this case, two kinds of resolution can be defined: The range resolution, which accounts for its ability to differentiate two objects on the same line-of-sight and is governed by pulse length (typically 3–4 mm

\* Corresponding author.

E-mail addresses: [camila.viana@usp.br](mailto:camila.viana@usp.br),  
[camila.duelis@gmail.com](mailto:camila.duelis@gmail.com) (C. Duelis Viana), [arthur.correia@usp.br](mailto:arthur.correia@usp.br) (A. Endlein),  
[ginaldo@usp.br](mailto:ginaldo@usp.br) (G. Ademar da Cruz Campanha),  
[guano@usp.br](mailto:guano@usp.br) (C. Henrique Grohmann).

The general workflow proposed in this paper can be seen in Fig. 2. Further information about each step is presented in the next sections. Herein we tested the algorithms to identify discontinuity planes ranging in size from a few decimeters to a few meters on irregular triangular meshes generated using SfM technique but, in principle, they can also be used to identify larger features such as rock layers and major faults on regularly spaced

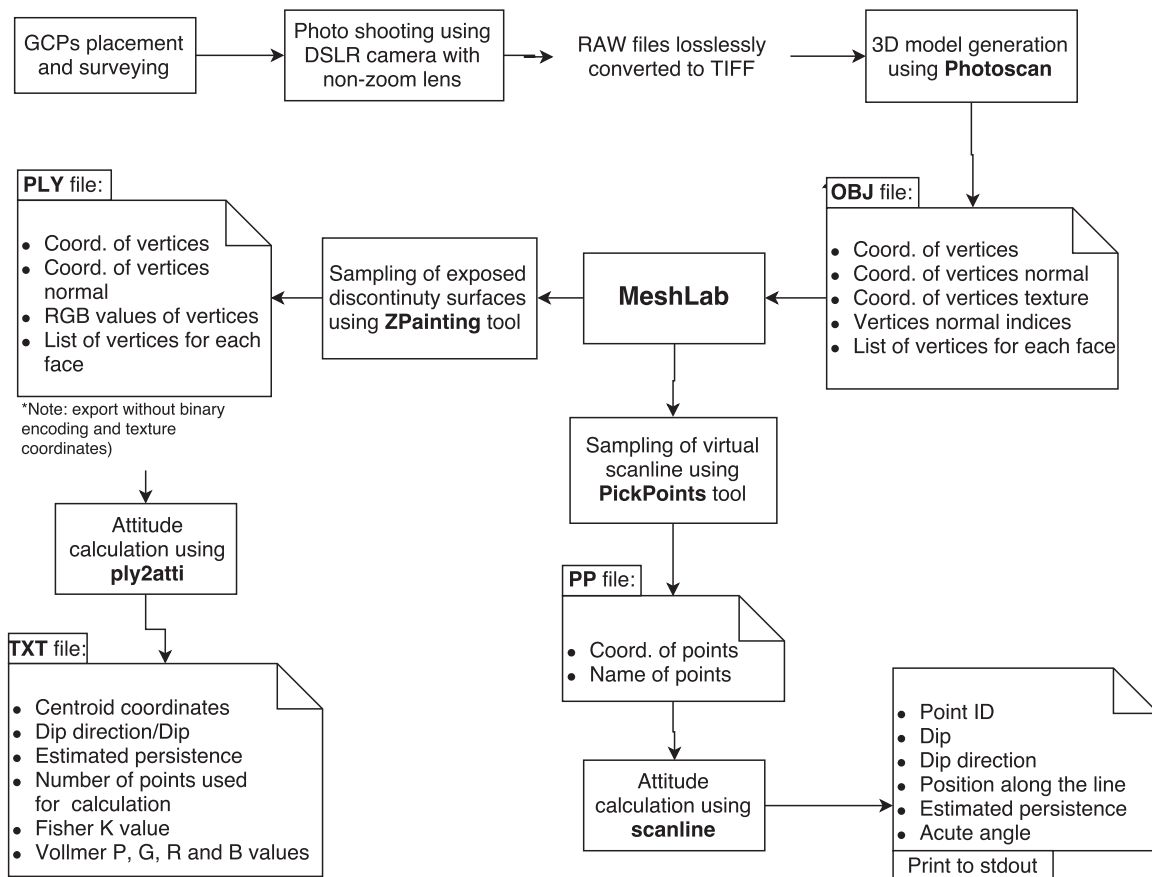


Fig. 2. Flow chart of general procedure adopted in this paper.

digital terrain models (DTM).

### 2.1. Site description

In order to compare traditional field compass measurements with virtually-obtained attitudes, two different sites were surveyed. The first one (Site 1) is composed of four wooden planes, used for didactical purposes, with different dip angles and surface areas, and a vertical concrete plane. They were arbitrarily placed within a local coordinate system created on an outdoor planar ground surface using a Cocla geological stratum compass and

adhesive tape to place the x, y, and z local axes parallel to East, North and vertical upwards, respectively. A measuring tape was used to mark 0.5 m spaced points on the axes (Fig. 3). These points were used for further georeferencing. The planes attitudes were measured with the Cocla geological stratum compass for control.

The second test site (Site 2) is a 130 m-long and 40 m-high metadolomite rock cut in an open pit quarry, located in Santana de Parnaíba city, São Paulo state, southeastern Brazil. For georeferencing, six ground control points (GCP) were placed on the rock cut and surveyed using a Topcon GPT-3200N reflectorless total station, which can provide a  $\pm(3 \text{ mm} + 2 \text{ ppm} \times D) \text{ m.s.e.}$

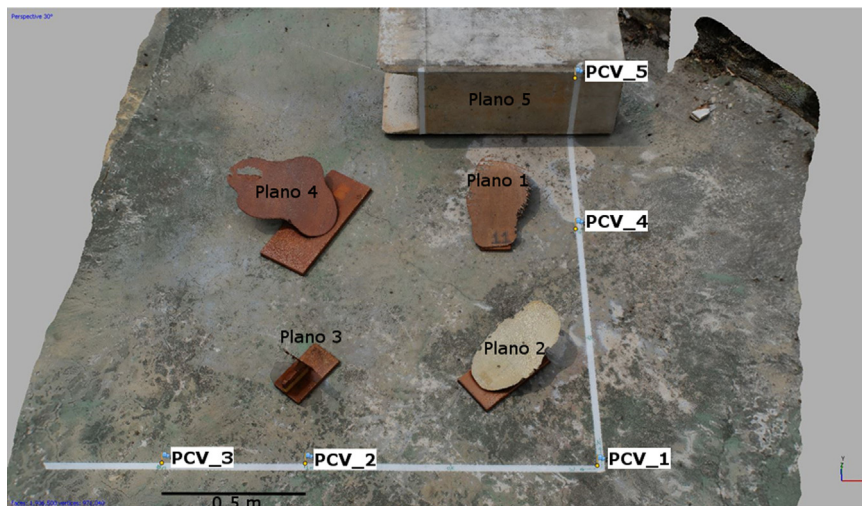


Fig. 3. Screenshot of Site 1 digital model. PCV labeled points indicate ground control points.



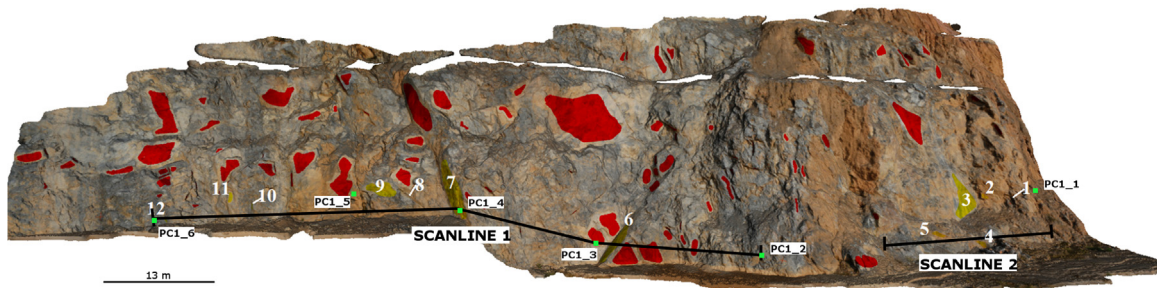


Fig. 4. Screenshot of Site 2 digital model with indication of the surveyed scanlines and individual planes. PC1 labeled points indicate ground control points.

accuracy. We measured two scanlines and twelve individual discontinuity surfaces in the field using a Coclá geological stratum compass (Fig. 4).

## 2.2. Photogrammetric models

The image acquisition was performed using a Nikon D200 digital camera with a 23.6 mm × 15.8 mm CCD sensor (3872 × 2592 pixels;  $PI=6.19$  microns) and a 28 mm focal length lens. The digital models were generated with Agisoft Photoscan professional edition (version 1.0.1) (Agisoft, 2014) a Structure-from-Motion based photogrammetric software. Further information about geological 3D digital models using Structure from Motion software can be found in Sturzenegger and Stead (2009) and Westoby et al. (2012). We first selected the best images based on scene relevance and image quality. No pre-calibration or post-mesh editing were performed. The processing options used and resulting model characteristics are shown in Table 1.

## 2.3. Algorithms

The algorithms were written in Python (Python Software Foundation, 2013), using the NumPy library (Oliphant, 2006) and the NetworkX package (Hagberg et al., 2008). Feature selection was made with MeshLab software (Cignoni et al., 2008). Both scripts are provided in Section 5.

### 2.3.1. Attitude calculation using vectors

Planar rock discontinuities representation by means of a unit vector parallel to their poles is very useful when processing this

type of data in computational environments, as they allow for easy manipulation. Considering the  $x$ ,  $y$ , and  $z$  axes referring, respectively, to East, North and vertical upwards, a plane with dip direction  $\alpha$  and dip  $\theta$  has the unit vector  $\mathbf{u}$  parallel to its pole described by Eq. (5). The transformation of the unit vector back to geological attitude is calculated according to Eqs. (6) and (7), comparing the sign to determine the dip direction quadrant.

$$\mathbf{u} = \begin{bmatrix} u_x \\ u_y \\ u_z \end{bmatrix} = \begin{bmatrix} \sin \alpha \sin \theta \\ \cos \alpha \sin \theta \\ \cos \theta \end{bmatrix} \quad (5)$$

$$\text{dip} = \arccos u_z \quad (6)$$

$$\text{dip}_{\text{dir}} = \arctan 2(u_x, u_y) \quad (7)$$

### 2.3.2. Scanline algorithm and workflow

The placement of a virtual scanline was made manually on MeshLab using the *PickPoints* tool. First, the start-end points of the line are placed by right clicking on their respective locations. Afterwards, for each individual recognizable surface and trace along the scanline that crosses it, three points are placed: two at start-end and one mid-point. The digital surface texture and high point density ensures that, even for traces, the three selected points for each feature are extremely unlikely to be collinear, allowing a “three-point problem” solution. The selected points are then exported on a XML file with .pp termination, which stores  $X$ ,  $Y$ , and  $Z$  coordinates of all the selected points – being scanline start-end points and three points per discontinuity – and point names (Fig. 5).

For each selected feature, considering three non-collinear points  $a$ ,  $b$  and  $c$ , a perpendicular resultant vector  $\mathbf{d}$  can be calculated from the cross product of a pair of the difference vectors between them, as shown in Eq. (8) and Fig. 6. The normalized  $\hat{\mathbf{d}}$  vector (unit vector) can then be used with Eqs. (6) and (7) to obtain the geological coordinates of the plane it represents (Eq. (9)). An approximate persistence value (discontinuity extent or length) is obtained as the magnitude of the largest difference vector between the three vectors.

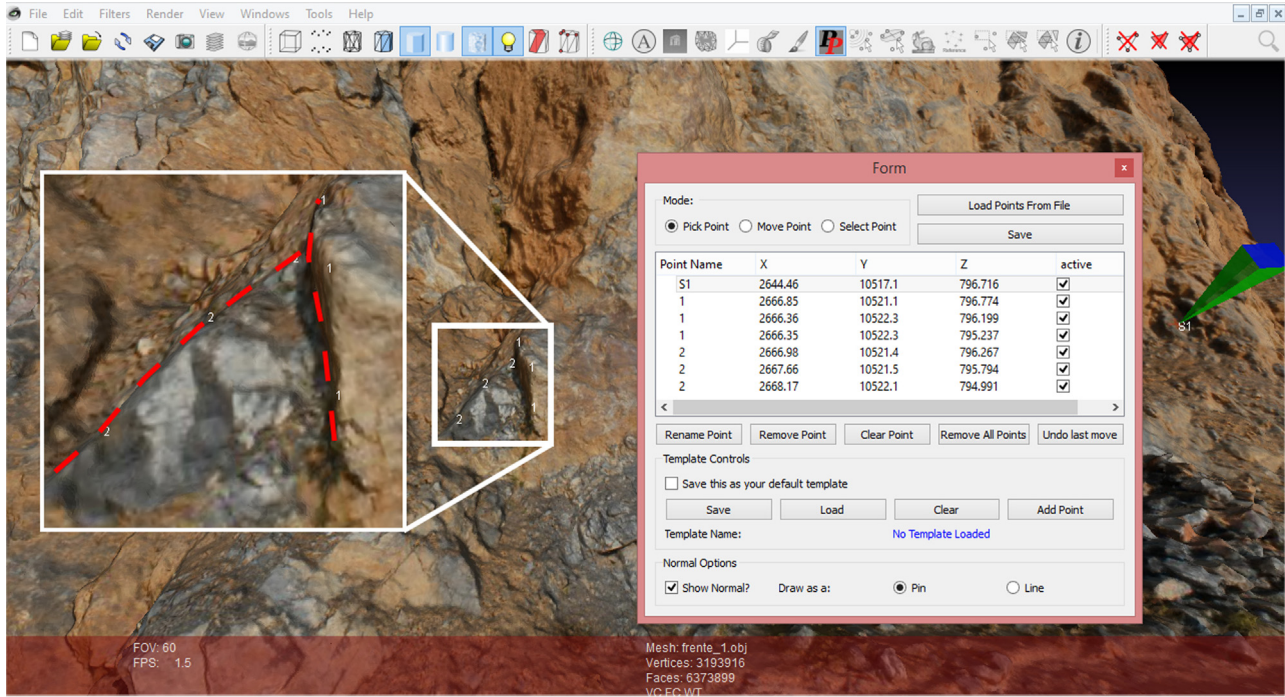
$$\mathbf{d} = (b - a) \times (c - a) \quad (8)$$

$$\hat{\mathbf{d}} = \frac{\mathbf{d}}{\|\mathbf{d}\|} \quad (9)$$

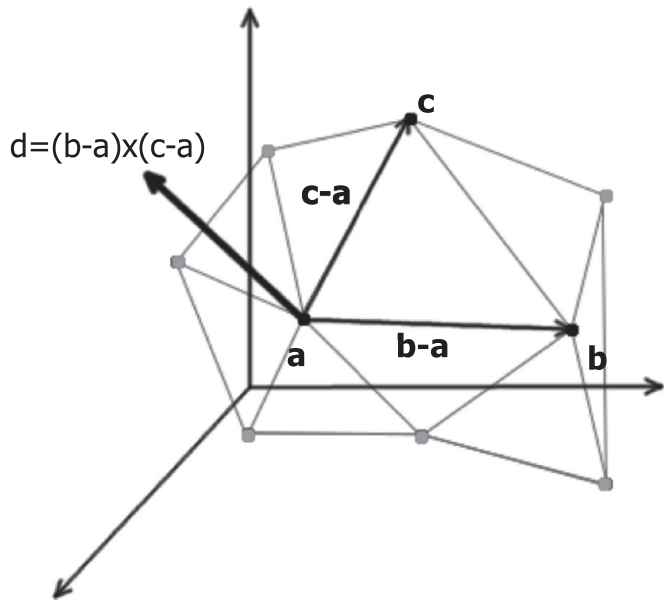
To calculate the discontinuity position  $p$  along the line, considering an  $ab$  scanline and the discontinuity centroid point  $c$ , found as the mean of the three points, the projection of the plane on the scanline is calculated according to Eq. (10). This procedure provides results similar to measurements performed during a field scanline survey, as it gives the discontinuity nearest position on the measure tape.

Table 1  
Characteristics and parameters set on Photoscan software for the digital models of Site 1 and Site 2.

	Site 1	Site 2
Number of images	58	78
Mean distance (m)	2.3	30.2
GSD (m)	0.0005	0.006
Error (pixel)	0.82	0.34
<b>Parameters for photo alignment</b>		
Accuracy	High	High
Pair selection	Disabled	Disabled
<b>Parameters for dense point cloud</b>		
Quality	Ultra high	Ultra high
Depth filtering mode	Aggressive	Aggressive
<b>Parameters for 3D mesh</b>		
Surface type	Arbitrary	Arbitrary
Source data	Dense cloud	Dense cloud
Polygon count	High	High
<b>Parameters for texturing</b>		
Mapping mode	Generic	Generic
Blending mode	Mosaic	Mosaic



**Fig. 5.** Screenshot of sampling procedure using PickPoints tool on MeshLab. The green prism indicates the scanline start point. On the zoomed image the dashed lines indicate the discontinuities and the white numbers (“1” and “2” indexes) show the three selected points for each plane, as they appear on the screen. (For interpretation of the references to color in this figure legend, the reader is referred to the web version of this article.)



**Fig. 6.** Calculation of the normal vector  $\hat{d}$  using three points ( $a$ ,  $b$  and  $c$ ) of a triangular mesh.

$$p = (c - a) \cdot \left( \frac{b - a}{\|b - a\|} \right) \quad (10)$$

### 2.3.3. ply2atti algorithm and workflow

The sampling of individual recognizable discontinuity surfaces on the 3D model is carried out in a different way. The digital measure of an extended surface on a digital model comprises a large number of points, unlike discrete compass measures at chosen locations (Sturzenegger and Stead, 2009). The virtual selection of the surfaces was made in MeshLab software using the .obj file of the 3D digital models generated on Photoscan. The .obj contains the vertex

coordinates, vertex normal coordinates, vertex texture coordinates, vertex normal indices and list of vertices for each face.

Each individual discontinuity plane was manually selected using the ZPainting tool, using it to color in the whole plane. To produce a pure color (i.e., with no transparency value) it is recommended to place the hardness setting on its maximum and to acquire greater precision it is possible to reduce the brush size according to the need. This procedure allows to classify different sets, based on geological or relevance criteria, using different colors during the selection. The RGB color values used in each selection are noted. For further processing, the painted digital model was exported in .ply file format, without binary encoding and texture coordinates. The .ply file contains the  $X, Y, Z$  coordinates,  $nX, nY, nZ$  normal coordinates and RGB values for each vertex, and the list of vertices that comprise each face of the mesh (Fig. 7).

The ply2atti algorithm selects from the whole mesh the vertices that have been painted with the given colors, building from these a graph, whose edges are built from the mesh faces information. Then, using a graph search algorithm it separates in individual planes each collection of vertices that share the same color and are connected by edges between vertices of the same color (connected components, in graph terminology). Given this, it is important to carefully select each plane so that neighboring surfaces do not share any connection. If so, they will be considered as an unique feature, as demonstrated in Fig. 8.

Considering a matrix comprising the vertices coordinates within the selected plane, the eigenvectors and eigenvalues of its covariance matrix (Eq. (11)) represent the axes and relative lengths of the dataset best-fit ellipsoid. Being  $\lambda_1 > \lambda_2 > \lambda_3$  the eigenvalues, three extreme shapes are expected: spherical for  $\lambda_1 = \lambda_2 = \lambda_3$ , planar for  $\lambda_1 = \lambda_2 \gg \lambda_3$  and linear for  $\lambda_1 \gg \lambda_2 = \lambda_3$ . Therefore, for planar discontinuities, the third eigenvector is parallel to the plane normal and, after being normalized, it can be used to calculate the geological attitude of the plane.

Given a geometric surface, the surface normal at a certain point



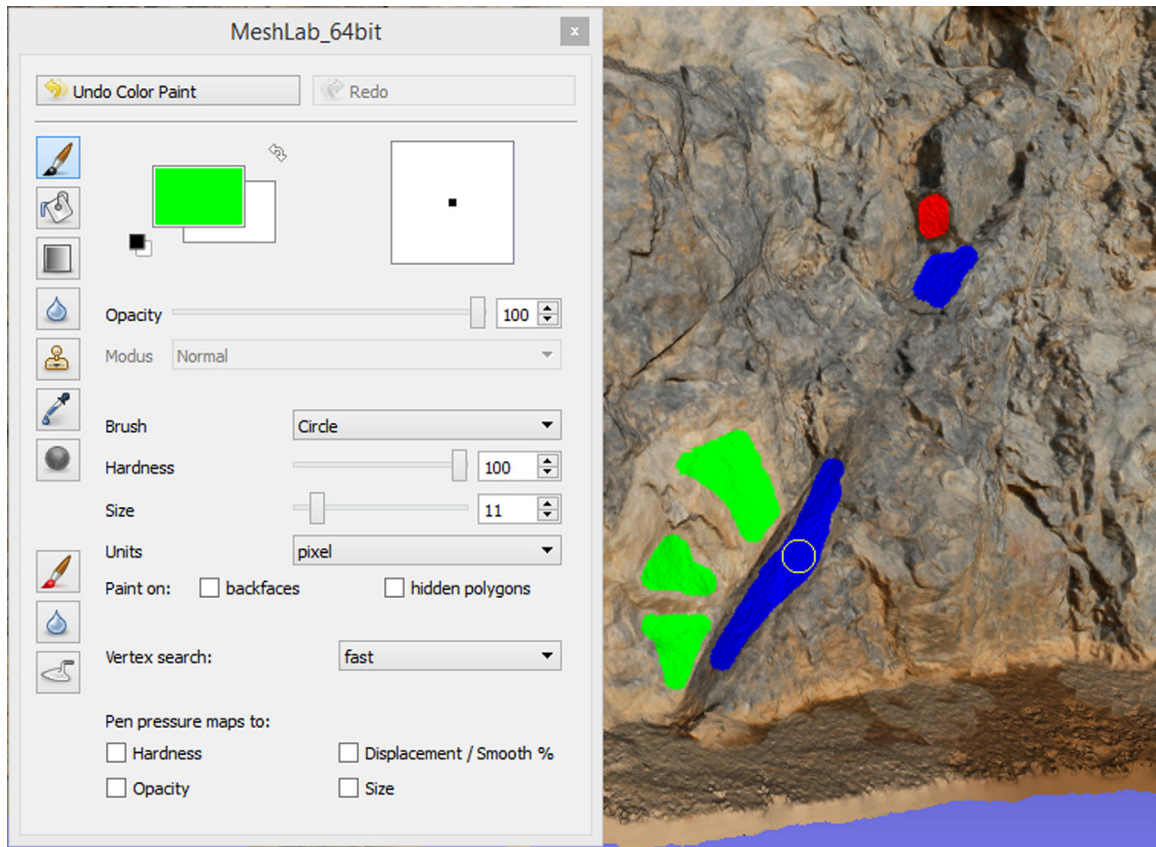


**Fig. 7.** Screenshot of sampling procedure using ZBrush tool on MeshLab. The white circle indicates the brush type and its size can be adjusted according to the plane extension to acquire greater precision. Interpreted sets are selected using different colors. In cases where the set identification is difficult, all planes can be selected using the same color, and the set interpretation made on a stereogram. (For interpretation of the references to color in this figure legend, the reader is referred to the web version of this article.)

is the vector perpendicular to the surface in that point. Numerically, for a set of  $N$  orientation data, Vollmer (1990) describes the expected shapes through three ratios (Eqs. (12)–(14)). They represent, respectively, the data set proximity to the punctual ( $P$ ), girdle ( $G$ ) and random ( $R$ ) distributions. If a perfectly flat surface is

composed by a set of points, the expected distribution for its  $N$  normals is punctual, as they are parallel one to another. The girdle distribution is expected for a wavy (or curved) surface, as a result of a dispersion of the surface normals and the random distribution, for example, for a spherical surface or, considering a point



**Fig. 8.** Example of plane selection using ZPainting tool on MeshLab. On the correct selection (left image) the four planes do not share any connections so they will be considered as four graphs. On the right image (wrong selection), planes 3 and 4 are connected, so the algorithm will process them as a single graph, giving a wrong attitude value.

cloud, a surface with noise data.

$$S = \frac{1}{n-1} \sum_{i=1}^n \begin{bmatrix} (x_i - \bar{x}) \cdot (x_i - \bar{x}) & (x_i - \bar{x}) \cdot (y_i - \bar{y}) & (x_i - \bar{x}) \cdot (z_i - \bar{z}) \\ (x_i - \bar{x}) \cdot (y_i - \bar{y}) & (y_i - \bar{y}) \cdot (y_i - \bar{y}) & (y_i - \bar{y}) \cdot (z_i - \bar{z}) \\ (x_i - \bar{x}) \cdot (z_i - \bar{z}) & (y_i - \bar{y}) \cdot (z_i - \bar{z}) & (z_i - \bar{z}) \cdot (z_i - \bar{z}) \end{bmatrix} \quad (11)$$

$$P = \frac{(\lambda_1 - \lambda_2)}{N} \quad (12)$$

$$G = \frac{2(\lambda_2 - \lambda_3)}{N} \quad (13)$$

$$R = \frac{3(\lambda_3)}{N} \quad (14)$$

The directional data statistics can be done by several means. Fisher (1953) presents the Fisher distribution for the tridimensional unit vector modeling on a sphere. This distribution, symmetric about the mean value, describes the angular distribution of orientations about a mean orientation vector. The probability density function is expressed by Eq. (15), where  $\theta$  is the angular deviation from the mean vector and  $K$  is the “Fisher constant”. The Fisher  $K$  express the tightness or dispersion of the orientations about the mean vector. For data sets larger than 30 vectors, the value can be estimated by Eq. (16), where  $N$  is the number of vectors and  $R$  is the length of the resultant vector.

$$f(\theta) = \frac{K \sin \theta e^{K \cos \theta}}{e^K - e^{-K}} \quad (15)$$

$$K \simeq \frac{N-1}{N-R} \quad (16)$$

The algorithm calculates the shape ratios and the Fisher  $K$  for the selected planes in order to guarantee that the selected features are planar. Additionally, the mean vector of the normal vectors belonging to each selected plane is calculated to give its centroid coordinates. An approximate persistence value is given calculating the distance between the extreme points for each plane.

#### 2.4. The user interface

For both scripts, the user interface is the command line. To calculate discontinuity attitudes using *ply2atti*, the user must type the script name followed by the input *.ply* file name, the desired output option and the RGB values of the color (or colors) used in feature selection. The *-n* option outputs each different colored plane in a single file (Ex. 1) and, in cases where multiple colors are used, the *-j* option stores all results in a single output file (Ex. 2).

To run the *scanline* algorithm the user must type on the command line the script name followed by the input *.pp* file name, as shown in Ex. 3. The resultant data is printed to stdout as: dip direction, dip, point ID, scanline distance, estimated persistence and the acute angle between the discontinuity and the scanline direction.

**Ex. 1.** > python ply2atti.py -f filename.ply -n R,G,B

**Ex. 2.** > python ply2atti.py -f filename.ply -j R1,G1,B1 R2,G2,B2

**Ex. 3.** > python scanline.py filename.pp

### 3. Results and discussion

#### 3.1. Site 1

The 3D digital model of the wooden planes was constructed from 58 photographs, and comprises 971,040 vertices and

1,936,500 faces (Fig. 3). The georeferencing total error is 0.005 m and the GSD is 0.0005 meters. The error obtained is very low considering the accuracy of scaling, which is influenced both by compass and measuring tape precision. Manual marker placement when registering images on Photoscan is also affected by the high model resolution as the targets were approximately 0.02 m high and 0.002 m wide, comprising about 160 pixels.

The five plane faces selected in MeshLab were processed using the *ply2atti* script and the results are presented in Table 2. The resulting data shows that the angular deviation between traditional compass measuring and digital attitudes is between 1° and 4°. The highest difference is associated to plane 3, which did not have its complete reconstruction (Fig. 9), possibly due to its steep dip (70°), reduced area and shadowing. Shape parameters (Fisher, 1953; Vollmer, 1990) indicate a punctual distribution of the vertices normal comprising the discontinuity surface, consistent with the expected for planar discontinuities.

#### 3.2. Site 2

The 3D digital model of the rock cut was constructed from 78 photographs, and comprises 3,193,916 vertices and 6,373,899 faces. The georeferencing total error is 0.03 m and the GSD 0.006 meters (Fig. 4). As on Site 1, the area of targets (approx.  $0.04 \times 0.04 \text{ m}^2$ ) may have influenced the accuracy of markers placed manually on Photoscan. The GCP distribution may also have affected this result since the targets were placed at the toe of the slope due to an access limitation. When registering images it is strongly recommended that the distribution of the GCP is uniform within the area. Another option for GCP placement is the printable coded targets available on Photoscan. Coded targets are printed markers that can be placed in the scene before photo shooting and are automatically recognized by Photoscan, allowing a more accurate and faster measurement of GCPs. The downside is that they are not weather resistant, so in the need of multiple photo sessions on different days the targets may move or be damaged, that is why we chose to paint the markers directly on the rock wall.

##### 3.2.1. Virtual linear sampling (scanline algorithm)

The virtual linear sampling was performed at the same locations of the field scanlines. Table 3 shows the frequency, mean spacing and theoretical RQD (RQD\*) (Priest and Hudson, 1976) results for the field and virtual surveys. The difference in the number of discontinuities measured by the two methods can be explained by the positioning of the field scanline, usually at the base of the slope, and thus too close to the digital model edges. Furthermore, discontinuities of limited extension may not be visible on the digital 3D model due to the spatial resolution of the photographs. For both survey methods, the RQD\* values (Deere and Deere, 1989) classify the rock mass as very good quality.

Considering virtual scanlines in different positions on the slope but with the same direction, the frequencies obtained are similar.

**Table 2**

Geological attitude of the selected planes on Site 1 measured with compass and calculated by *ply2atti* algorithm. Angular deviation between measures, number of digital model faces used for the calculation and shape ratios are included.

Plane	Compass reading	Digital attitude	Angular deviation (deg)	Number of faces	K	P	G	R
1	183/10	182/08	2.006	4733	579.77	0.99	0.01	0.00
2	235/20	232/20	1.026	7885	1042.81	1.00	0.00	0.00
3	040/70	035/71	4.818	338	44.53	0.93	0.02	0.05
4	133/20	135/17	3.006	9903	530.44	0.99	0.00	0.00
5	180/90	179/88	2.236	29,024	100.01	0.96	0.02	0.02



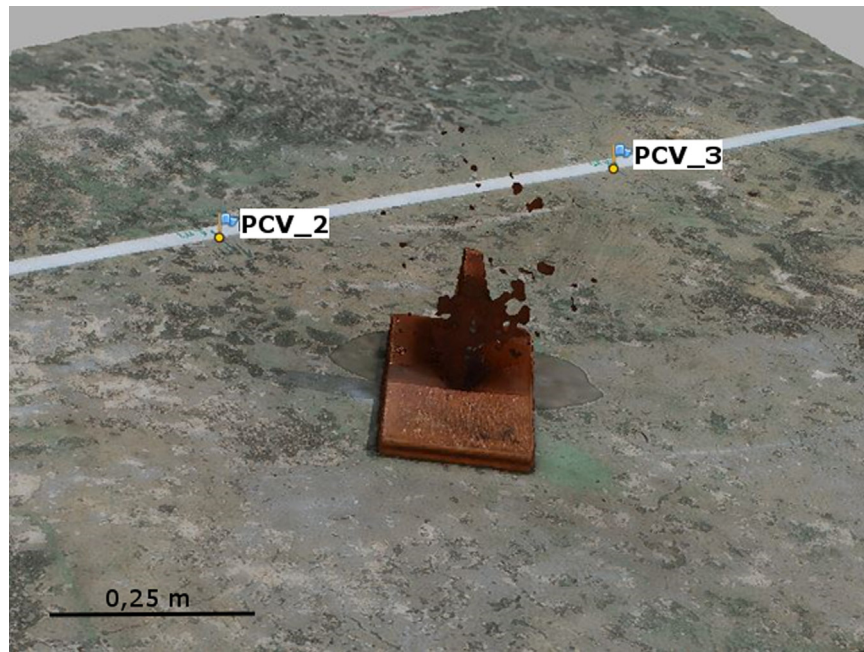


Fig. 9. Detail of reconstruction failure of plane 3 in Site 1 digital model. PCV labeled points indicate ground control points.

**Table 3**

Calculated parameters for total data resulting from traditional field scanlines and virtual line sampling.

	Scanline 1		Scanline 2	
	Field	Virtual	Field	Virtual
Frequency (joint/m)	0.273	0.441	2.749	0.490
Mean spacing (m)	3.664	2.267	0.364	2.041
RQD* 0.1 m (%)	99.963	99.91	96.847	99.88
RQD* 0.3 m (%)	99.682	99.20	79.968	99.02
RQD* 1.0 m (%)	96.888	92.71	23.998	91.28
Number of poles	40	33	48	10

However, the virtual frequency value for Scanline 2 was much smaller than that obtained by the field survey. This difference suggests a limitation imposed by the photographs spatial resolution, causing a lack of sensitivity to very small or less-persistent discontinuities along the virtual sampling lines. For example, considering the GSD, a discontinuity with a 0.1 m persistence appears on the image as 17 pixels, making it difficult to be visually identified and so lowering the count of discontinuities per meter.

The discontinuity measures obtained by virtual and field sampling (Fig. 10) were classified into attitude sets by cluster analysis using DIPS software, version 6.0 (Rocscience, 2013). At first sight the identified sets are the same for both methods (Fig. 11). The angular deviation between the mean pole planes of the same set by each method were calculated (Table 4). The angular deviations range from 14.03° to 23.23°. A possible explanation is the strong scatter of measures of the studied rock mass. The discontinuity surfaces are often irregular and wavy, which makes a cluster analysis difficult and causes the attitudes obtained by the virtual sampling to represent a mean surface of the discontinuity, unlike the discrete field compass measures.

The calculated parameters for the sets present no significant differences on frequency and spacing values obtained by virtual and field sampling. Virtual linear sampling presented larger persistence values. Persistence remains one of the most difficult rock mass parameters to quantify in field scanline surveys (ISRM, 1978), so the values obtained on the traditional field sampling may be underestimated.

### 3.2.2. Individual planes (ply2atti algorithm)

Twelve individual recognizable discontinuity planes were selected using MeshLab and processed using *ply2atti* algorithm and its attitudes were also taken in the field with magnetic compass. The results are presented in Table 5. We observed an angular deviation ranging from 4° to 29° between the field compass measure and the virtual measures. The larger deviations are associated to: irregularity and curviness of the real discontinuity surface on planes 2, 7 and 11; distortion of the digital generated surface on planes 4 and 5; little persistent and very oblique discontinuity on plane 12. In very irregular discontinuities surfaces the angular deviation can be understood as a sampling/data fitting difference. In such cases, a single measure taken with a compass represents a small fraction of the total surface, while digitally obtained attitudes are a mean value of the whole surface.

The differences associated to distortions on the generated digital surface can be avoided with pre- or post-processing for noise removal. In addition, discontinuities close to the 3D digital model edges, where there is larger surface distortion, should be avoided.

As discussed in Section 2, for planar discontinuities we expected that the angular deviations between field and virtual measurements would be smaller for near punctual data distributions. We observed that even for wavy surfaces (e.g., plane 11) the *P* value is near 1. These results show that the use of the four eigenvalue-based indexes proposed by Vollmer (1990) to assist in discriminating distribution of a data set do not apply to real wavy and irregular surfaces as a measure of flatness. It can be assumed that the dispersion given to the surface normals of a wavy discontinuity plane is not significant enough to be identified in the orientation data distribution, thus the visual inspection of the discontinuity surface during the virtual sampling is necessary to identify irregular/distorted planes.

It must be pointed out that there is a difference between the data provided by the field scanline survey and the photogrammetric approach. The digital model favors the sampling of those planes parallel or near-parallel to the free rock face, perpendicular to the line of sight of the camera. On the other hand, the field scanline technique favors those planes perpendicular or near-perpendicular to the scanline direction. This variation may affect data density provided by both methods and the identification of



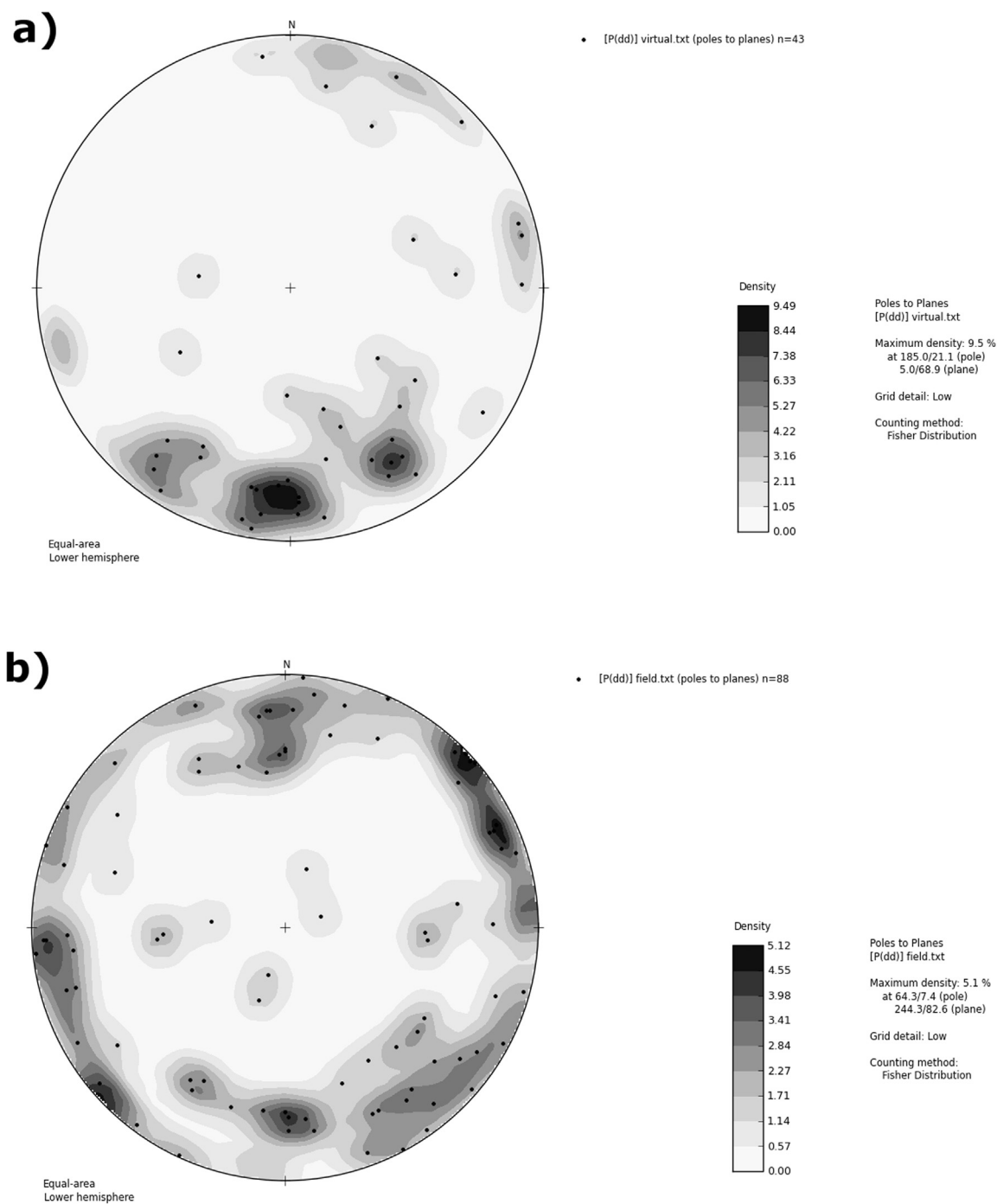


**Fig. 10.** Stereographic projection of: (a) 43 poles obtained by virtual line sampling and (b) 88 poles obtained by traditional field line sampling. Schmidt–Lambert diagram, lower hemisphere.

discontinuity sets. Therefore, it can be of great value to jointly analyze the data, applying a weighting to account the sampling bias introduced by orientation data collecting by both methods.

The accuracy and quality of the 3D model influences on the results. The smaller angular deviations observed are associated with the more detailed model (Site 1, smaller GSD). Considering the same surface area imaged at two different settings, the one with the smaller resultant GSD will generate a 3D surface with a higher number of points (more detailed) and, therefore, suitable for a best fitting. This observation points to a need of planning the image acquisition based on the size of the smallest feature the user wants to be visible on the 3D model.

#### 4. Conclusions

The application of the developed method was successful. The comparison between the traditional field magnetic compass measures and virtual sampling over 3D photogrammetric-based digital models shows that the latter is reliable.

Attitude measurements of individual planes both by virtual and field techniques, on artificial models and on real complex outcrop, show consistent results. The identification of fractures sets, its frequency and persistency show some significant differences, which can be partially explained by the greater extensiveness of the photogrammetric survey over a large outcrop compared with the more localized field measurements with a compass.

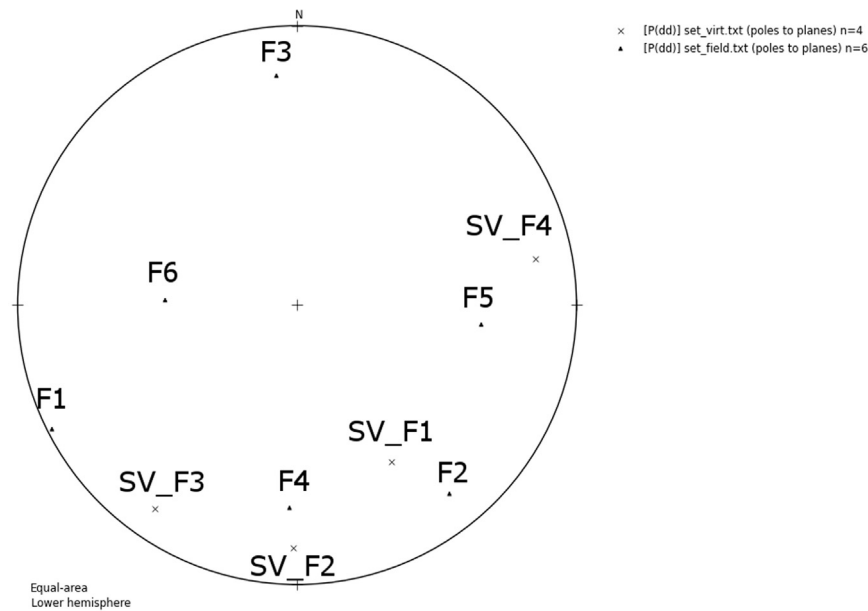


**Fig. 11.** Stereographic projection of mean attitude of joint sets obtained by traditional scanlines (triangles) and virtual line sampling (crosses). Schmidt–Lambert diagram, lower hemisphere.

**Table 4**

Comparison between joint set properties for the virtual mean set orientations (SV) and traditional sampling mean set (F) orientations.

Sets (virtual//field)	SV_F1//F2	SV_F2// F4	SV_F4//F5
Angular deviation (deg)	14.03	22.20	25.23
Frequency (joint/m)	0.136//0.147	0.126//0.090	0.052//0.049
Mean spacing (m)	7.331//6.805	7.942//11.136	19.060//20.417
Persistence (m)	1–5//1–3	0.5–7//<1	1–6//1–3

**Table 5**

Geological attitude of the selected planes on Site 2 measured with compass and calculated by *ply2atti* algorithm. Angular deviation between measures, number of digital model faces used for the calculation and shape ratios are included.

Plane	Compass reading	Digital attitude	Angular deviation (deg)	Number of faces	K	P	G	R
1	220/28	232/28	5.626	40	23.82	0.85	0.14	0.01
2	352/87	008/86	16.001	330	26.11	0.88	0.05	0.07
3	320/73	333/71	12.521	6686	60.76	0.95	0.01	0.04
4	224/82	202/89	23.001	255	62.57	0.95	0.03	0.02
5	160/72	187/86	29.901	411	53.58	0.94	0.01	0.05
6	085/42	063/40	14.517	3918	77.33	0.96	0.02	0.02
7	048/83	029/82	18.862	7960	30.38	0.90	0.02	0.07
8	210/59	208/52	7.191	33	81.17	0.96	0.04	0.00
9	339/76	348/82	10.675	1802	26.67	0.88	0.04	0.07
10	040/81	035/81	4.938	84	80.07	0.96	0.03	0.01
11	334/85	357/71	26.438	190	62.20	0.94	0.04	0.02
12	006/72	008/88	16.120	66	24.15	0.87	0.07	0.06

The virtual measurements can be affected by factors such as the photo-resolution, distortions at the edges of the model and shadowing. Besides the general recommendations for good quality SfM photogrammetric images (non-zoom camera lens, fixed focus length, good camera resolution, manual control, good light conditions, multiple views) we also recommend the planning of the photo-surveying taking into account the needed level of detail to avoid under-sampling due to ground resolution. Both virtual and field approaches are affected by the planes orientations about the point of view or the outcrop direction, but in different ways. The photogrammetric approach favors planes parallel to the outcrop

while the field scanline technique, those perpendicular to the outcrop.

## 5. Supplementary material

Supplementary data related to this article can be found at <http://git.io/vqVHO> under a Creative Commons CCO 1.0 Universal License.

## Acknowledgments

The authors would like to sincerely thank Prof. Frank Fueten and an anonymous referee for their careful reviews and FAPESP (2013/15862-8), the graduate program in Geochemistry and Geotectonics (IGc-USP) for financial support, and CNPq for a research fellowship to C.D. Viana (133050/2013-0). G.A.C. Campanha was supported by CNPq (302481/2012) and C.H. Grohmann was supported by CNPq (306294/2012-5) and FAPESP (2009/17675-5). Special thanks to the Geocal Mining team and support.

## References

- Agisoft, 2014. Agisoft Photoscan User Manual. ([http://www.agisoft.com/pdf/photo-scan-pro\\_1\\_1\\_en.pdf](http://www.agisoft.com/pdf/photo-scan-pro_1_1_en.pdf)).
- Assali, P., Grussenmeyer, P., Villemin, T., Pollet, N., Viguier, F., 2014. Surveying and modeling of rock discontinuities by terrestrial laser scanning and photogrammetry: semi-automatic approaches for linear outcrop inspection. *J. Struct. Geol.* 66, 102–114. <http://dx.doi.org/10.1016/j.jsg.2014.05.014> <http://linkinghub.elsevier.com/retrieve/pii/S0191814114001187>.
- Cignoni, P., Corsini, M., Ranzuglia, G., 2008. Meshlab: an open-source 3d mesh processing system. *ERCIM News* 73, 45–46. <http://ercim-news.ercim.eu/en73/rd/meshlab-an-open-source-3d-mesh-processing-system>.
- Deere, D.U., Deere, D.W., 1989. Rock Quality Designation (RQD) after Twenty Years. Technical Report. DTIC Document.
- Fisher, R.A., 1953. Dispersion on a sphere. *Proc. R. Soc. Lond. A17*, 295–305.
- Hagberg, A., Swart, P., Schult, D., 2008. Exploring network structure, dynamics, and function using NetworkX. In: *Proceedings of the 7th Python in Science Conference (SciPy 2008)*, pp. 11–16.
- Haneberg, W.C., 2008. Using close range terrestrial digital photogrammetry for 3-D rock slope modeling and discontinuity mapping in the United States. *Bull. Eng. Geol. Environ.* 67, 457–469. <http://dx.doi.org/10.1007/s10064-008-0157-y>, <http://link.springer.com/10.1007/s10064-008-0157-y>.

- ISRM, 1978. Suggested methods for the quantitative description of discontinuities in rock masses. *Int. J. Rock Mech. Min. Sci. Geomech. Abstr.* 15, 319–368.
- Moulon, P., Bezzi, A., 2012. Python Photogrammetry Toolbox: A Free Solution for Three-dimensional Documentation. In: *Archeofoss, VI Workshop*, Napoli, pp. 153–170.
- Oliphant, T., 2006. *Guide to NumPy*. Trelgol Publishing, USA. <http://web.mit.edu/dvp/Public/numpybook.pdf>.
- Pesci, A., Teza, G., Bonali, E., 2011. Terrestrial laser scanner resolution: numerical simulations and experiments on spatial sampling optimization. *Remote Sens.* 3, 167–184.
- Priest, S., Hudson, J., 1976. Discontinuity spacings in rock. *Int. J. Rock Mech. Min. Sci. Geomech. Abstr.* 13, 135–148. [http://dx.doi.org/10.1016/0148-9062\(76\)90818-4](http://dx.doi.org/10.1016/0148-9062(76)90818-4) <http://www.sciencedirect.com/science/article/pii/0148906276908184>.
- Priest, S., Hudson, J., 1981. Estimation of discontinuity spacing and trace length using scanline surveys. *Int. J. Rock Mech. Min. Sci. Geomech. Abstr.* 18, 183–197.
- Python Software Foundation, 2013. *Python Programming Language*, version 2.7. Available at (<http://www.python.org/>) (accessed 15.08.13).
- Rocscience, 2013. *Dips* 6.0.
- Sturzenegger, M., Stead, D., 2009. Close-range terrestrial digital photogrammetry and terrestrial laser scanning for discontinuity characterization on rock cuts. *Eng. Geol.* 106, 163–182. <http://dx.doi.org/10.1016/j.enggeo.2009.03.004> <http://linkinghub.elsevier.com/retrieve/pii/S0013795209000556>.
- Tavani, S., Granado, P., Corradetti, a., Girundo, M., Iannace, a., Arbués, P., Muñoz, J., Mazzoli, S., 2014. Building a virtual outcrop, extracting geological information from it, and sharing the results in Google Earth via OpenPlot and Photoscan: an example from the Khaviz Anticline (Iran). *Comput. Geosci.* 63, 44–53. <http://dx.doi.org/10.1016/j.cageo.2013.10.013> <http://linkinghub.elsevier.com/retrieve/pii/S009830041300277X>.
- Terzaghi, R.D., 1965. Sources of error in joint surveys. *Geotechnique* 15, 287–304. <http://dx.doi.org/10.1680/geot.1965.15.3.287>.
- Vasuki, Y., Holden, E.J., Kovesi, P., Micklethwaite, S., 2014. Semi-automatic mapping of geological Structures using UAV-based photogrammetric data: an image analysis approach. *Comput. Geosci.* 69, 22–32. <http://dx.doi.org/10.1016/j.cageo.2014.04.012> <http://linkinghub.elsevier.com/retrieve/pii/S0098300414000892>.
- Vollmer, F.W., 1990. An application of eigenvalue methods to structural domain analysis. *Geol. Soc. Am. Bull.* 102, 786–791 (<http://gsabulletin.gsapubs.org/content/102/6/786.full.pdf+html>).
- Westoby, M.J., Brasington, J., Glasser, N.F., Hambrey, M.J., Reynolds, J.M., 2012. 'Structure-from-Motion' photogrammetry: a low-cost, effective tool for geoscience applications. *Geomorphology* 179, 300–314. <http://dx.doi.org/10.1016/j.geomorph.2012.08.021>, <http://www.sciencedirect.com/science/article/pii/S0169555X12004217>.
- Wu, C., 2013. Towards linear-time incremental structure from motion. In: *Proceedings of the International Conference on 3D Vision – 3DV, 2013*, pp. 127–134. doi: 10.530 1109/3DV.2013.25.
- Wu, C., Agarwal, S., Curless, B., Seitz, S.M., 2011. Multicore bundle adjustment. In: *Proceedings of the IEEE Conference on Computer Vision and Pattern Recognition (CVPR)*, pp. 3057–3064.